

Article

A Study of Support Effects for the Water-Gas-Shift Reaction over Cu

Jian Chang , Zhuoming Feng, John M. Vohs  and Raymond J. Gorte * 

Department of Chemical and Biomolecular Engineering, University of Pennsylvania, Philadelphia, PA 19104, USA
* Correspondence: gorte@seas.upenn.edu; Tel.: +1-215-898-4439

Abstract: The water–gas–shift (WGS) reaction was studied on a series of supported Cu catalysts in which the MgAl_2O_4 (MAO) support was modified by depositing ZnO, CeO_2 , Mn_2O_3 and CoO using Atomic Layer Deposition (ALD). Addition of Cu by one ALD cycle gave rise to catalysts with nominally 1-wt% Cu. A 1.1-wt% Cu/MAO catalyst prepared by ALD exhibited twice the dispersion but ten times the WGS activity of a 1-wt% Cu/MAO catalyst prepared by impregnation, implying that the reaction is structure sensitive. However, Cu catalysts prepared with the ZnO, CeO_2 , and Mn_2O_3 films showed negligible differences from that of the Cu/MAO catalyst, implying that these oxides did not promote the reaction. Cu catalysts prepared on the CoO film showed a slightly lower activity, possibly due to alloy formation. The implications of these results for the development of better WGS catalysts is discussed.

Keywords: water–gas–shift; copper; support effects; atomic layer deposition



Citation: Chang, J.; Feng, Z.; Vohs, J.M.; Gorte, R.J. A Study of Support Effects for the Water-Gas-Shift Reaction over Cu. *Catalysts* **2022**, *12*, 1364. <https://doi.org/10.3390/catal12111364>

Academic Editors: Keith Hohn, Kotohiro Nomura, Evangelos Topakas, Vincenzo Baglio, C. Heath Turner, Leonarda Liotta, Jean-François Lamonier and Maria A. Goula

Received: 2 October 2022

Accepted: 31 October 2022

Published: 4 November 2022

Publisher's Note: MDPI stays neutral with regard to jurisdictional claims in published maps and institutional affiliations.



Copyright: © 2022 by the authors. Licensee MDPI, Basel, Switzerland. This article is an open access article distributed under the terms and conditions of the Creative Commons Attribution (CC BY) license (<https://creativecommons.org/licenses/by/4.0/>).

1. Introduction

The water–gas–shift (WGS) reaction, $\text{CO} + \text{H}_2\text{O} = \text{CO}_2 + \text{H}_2$, is critically important for maximizing the production of H_2 from syngas [1]. Because rates increase with temperature and equilibrium is favored at lower temperatures, the reaction is traditionally carried out in two stages in large-scale H_2 plants, using a high-temperature, Fe_3O_4 -based catalyst at higher temperatures in the initial stage and a Cu-based catalyst at lower temperatures to increase the yield. Although the catalysts for these processes have been in use for many years, there is still significant ongoing work to develop new materials, particularly for operation in smaller fuel processors, where one would like to use a single catalyst for both high- and low-temperature operation [2,3]. The traditional Fe_3O_4 -based catalysts are not sufficiently active at low temperatures and Cu-based catalysts tend to sinter at higher temperatures [4].

One method for increasing both activity and stability of metal catalysts for WGS involves changing the support. For example, ceria-supported, group 10 metals (e.g., Ni, Pd, and Pt) exhibit much higher WGS rates than their alumina-supported counterparts due to oxygen transfer at the metal-ceria interface [5]. Because reduced ceria is easily oxidized by water and oxidized ceria can transfer oxygen to the group 10 metals for CO oxidation, rates on these catalysts can be orders of magnitude higher than that observed on either ceria or the group 10 metals individually [6–9]. A similar mechanism may be responsible for high rates on titania-supported metals [10–12].

Cu is different from the group 10 metals in that oxidation of metallic Cu by H_2O is more thermodynamically favorable [13]. Therefore, dissociation of water occurs more easily on the metal itself, making the need for a promoter, like ceria, less obvious [14]. The conventional support for Cu-based WGS catalysts is Al_2O_3 , along with added ZnO [4]. The Al_2O_3 simply provides surface area and is not expected to modify the catalytic properties of Cu. The role of ZnO is less clear but its role appears to be primarily that of a getter to prevent sulfur poisoning [4]. However, it should be noted that Zn alloy formation has

been reported to enhance WGS rates with Pd [15]. While alloy formation is probably not important under WGS conditions for Cu/ZnO/Al₂O₃ catalysts, other kinds of Cu-ZnO interactions cannot be ruled out [16].

There is evidence that oxides other than ZnO can affect the activity of Cu for the WGS reaction [17–21]. A number of studies have indicated promotion by CeO₂ [17,18,22,23], likely for similar reasons as with the group 10 metals [8]. MnO_x has also been suggested as a promoter for WGS over Cu. For example, Tanaka et al. prepared a CuMn₂O₄ catalyst by coprecipitation and found its activity to be similar to Cu/ZnO/Al₂O₃ despite having a much lower surface area [24]. Similarly, Tabakova et al. reported that a Cu-Mn spinel showed high activity and stability [25]. Finally, WGS promotion by Co has been reported by several groups [26–28]. While these latter studies suggest that the catalyst is a Cu-Co alloy, thermodynamic measurements on small Co particles imply that the Co may be present as an oxide under WGS conditions [29].

The mechanisms by which a support affects WGS activity are likely support dependent. As discussed above, the support could itself be a promoter that assists the dissociation of water. In other cases, the support simply modifies the adsorption and reaction properties of the metal. For example, with very small particles, the support can change the average oxidation state of the metal atoms by transfer of electrons [30], which in turn would affect the adsorption and reaction properties. Alternatively, the support could simply influence the shape, and therefore the exposed surface facets, of the metal particles. Studies have shown that Cu can wet ZnO surfaces under some conditions [1,31], implying that ZnO can affect Cu particles shapes; and this could well affect rates since the WGS reaction over Cu has been reported by some to be particle-size dependent [19,32]. In a related example, studies of Pt supported on ZnO crystals have also demonstrated that ZnO can modify the shape and adsorption properties of the metal [33].

One difficulty with studies of support effects is that oxides used as supports have different surface areas and surface textures, making it difficult to isolate chemical effects from these other physical factors. When the oxide of interest is added to an inert support (e.g., ZnO onto Al₂O₃ in the case of WGS catalysts.), contact between the metal catalyst and the oxide promoter is not assured [34]. Therefore, in order to minimize the effects of surface area and oxide morphology while ensuring contact between the catalytic metal and the oxide of interest, our research groups have examined supported-metal catalysts in which the oxides of interest are deposited as conformal films onto an inert support using Atomic Layer Deposition (ALD) [35]. The ALD films are produced by first exposing the inert support to a gas-phase precursor of the desired oxide, after which the adsorbed precursor is oxidized in a separate step. This procedure is repeated as often as necessary to achieve a conformal oxide film with the desired thickness. Using this method, a series of catalyst supports can be prepared that have different surface compositions but nearly the same surface area and morphology.

In the present study, we have studied the effects of the support composition on Cu for the WGS reaction using thin films of ZnO, Mn₂O₃, CeO₂, and CoO on MgAl₂O₄ (MAO). MAO was chosen because of its low reactivity with the oxide films. Although WGS rates were found to be significantly higher when Cu was added to these supports by ALD, rather than conventional impregnation, all of the fresh catalysts showed similar rates, with the exception of the CoO-based catalyst, which was less active, probably due to alloy formation.

2. Results and Discussion

2.1. Characterization of Supports

A list of the catalyst supports used in this study, together with some of their properties, is shown in Table 1. The supports were formed by depositing 20 ALD cycles of the various oxides onto the MAO substrate. As shown in Figure 1, the oxide coverages were measured gravimetrically after every 5 ALD cycles. The film thicknesses and growth rates in Table 1 were then calculated by assuming the films grew uniformly and had the same density as that of the bulk oxides. The growth rates for each of the four oxides was between 0.009 and

0.02 nm/cycle, values that are in reasonable agreement with typical growth rates reported in the literature for precursors with large ligands [36]. The growth rates for CeO₂, Mn₂O₃, CoO were also identical to that observed previously in our laboratories on Al₂O₃ [35]. As shown in Table 1, the BET surface areas of the supports decreased upon the addition of the films. This is primarily due to an increase in the sample mass, leading to a decrease in the surface area per mass. Because the ALD films were so thin, the pore volume and average pore diameter will not change.

Table 1. Properties of the ALD-modified supports used in this study.

Sample	Thickness Growth Rate (nm/cycle)	Final Metal Oxide Weight Loading (%)	Final Film Thickness (nm)	BET Surface Area (m ² /g)
MgAl ₂ O ₄ (MAO) *	–	–	–	95
ZnO/MAO	0.020	23	0.41	60
CeO ₂ /MAO	0.018	24	0.36	77
Mn ₂ O ₃ /MAO	0.018	18	0.35	86
CoO/MAO	0.009	10	0.19	74

* MAO has a pore volume of 0.0030 cm³/g, and an average pore diameter of 7.8 nm.

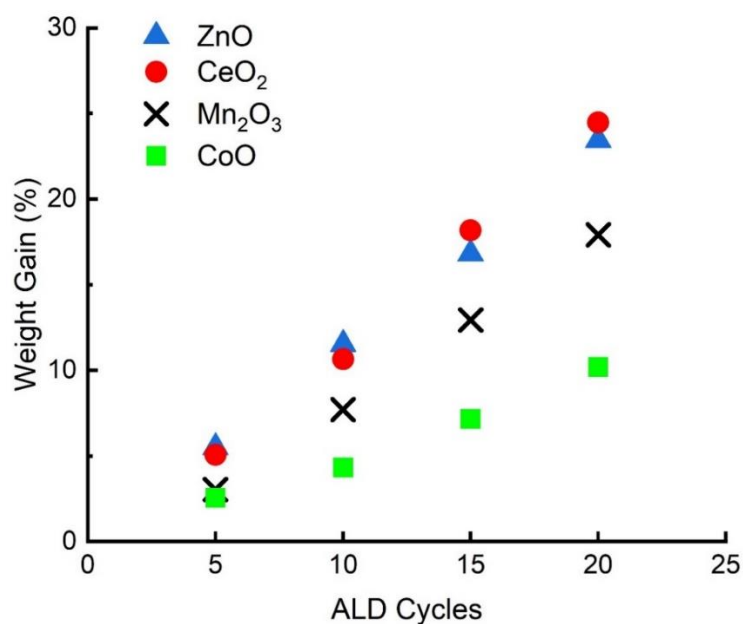


Figure 1. ALD Growth rates for the various oxides on MAO.

STEM-EDS measurements were performed on the ALD-modified supports to determine whether the films covered the MAO uniformly. These are reported in Figure 2a–d). The STEM images in each case were indistinguishable from that of the initial MAO, implying that the added films did not change the overall morphology of the samples. More importantly, the EDS maps of the elements showed a good correspondence between the overlayer oxides and the underlying Al signal from the MAO. Therefore, the overlayer compositions must be uniform on the 10-nm scale shown in the images.

TPD-TGA with adsorbed 2-propanol is a more sensitive method for determining the surface composition of mixed oxides because the temperature at which 2-propanol undergoes dehydration depends on the Lewis acidity of the oxide onto which the alcohol is adsorbed [37,38]; therefore, TPD-TGA experiments were performed for each of the supports used in this study, with results shown in Figure 3. After exposing the fresh MAO to 2-propanol vapor at room temperature, followed by evacuation for 1 h, the adsorbate coverage was approximately 580 μmol 2-propanol/g of support, or 3.7×10^{18} molecules/m² (Figure 3a). This specific coverage is close to what would be expected for a close-packed

monolayer of 2-propanol, implying that the entire surface was covered. Upon ramping the temperature, about half of the 2-propanol ($m/e = 45$) desorbs unreacted below 450 K, with the rest desorbing as propene ($m/e = 41$) in a sharp peak centered at 500 K and water. (The signal for water is not shown here because it desorbs over a wide temperature range.) After heating to 800 K, the sample mass returned to its initial value.

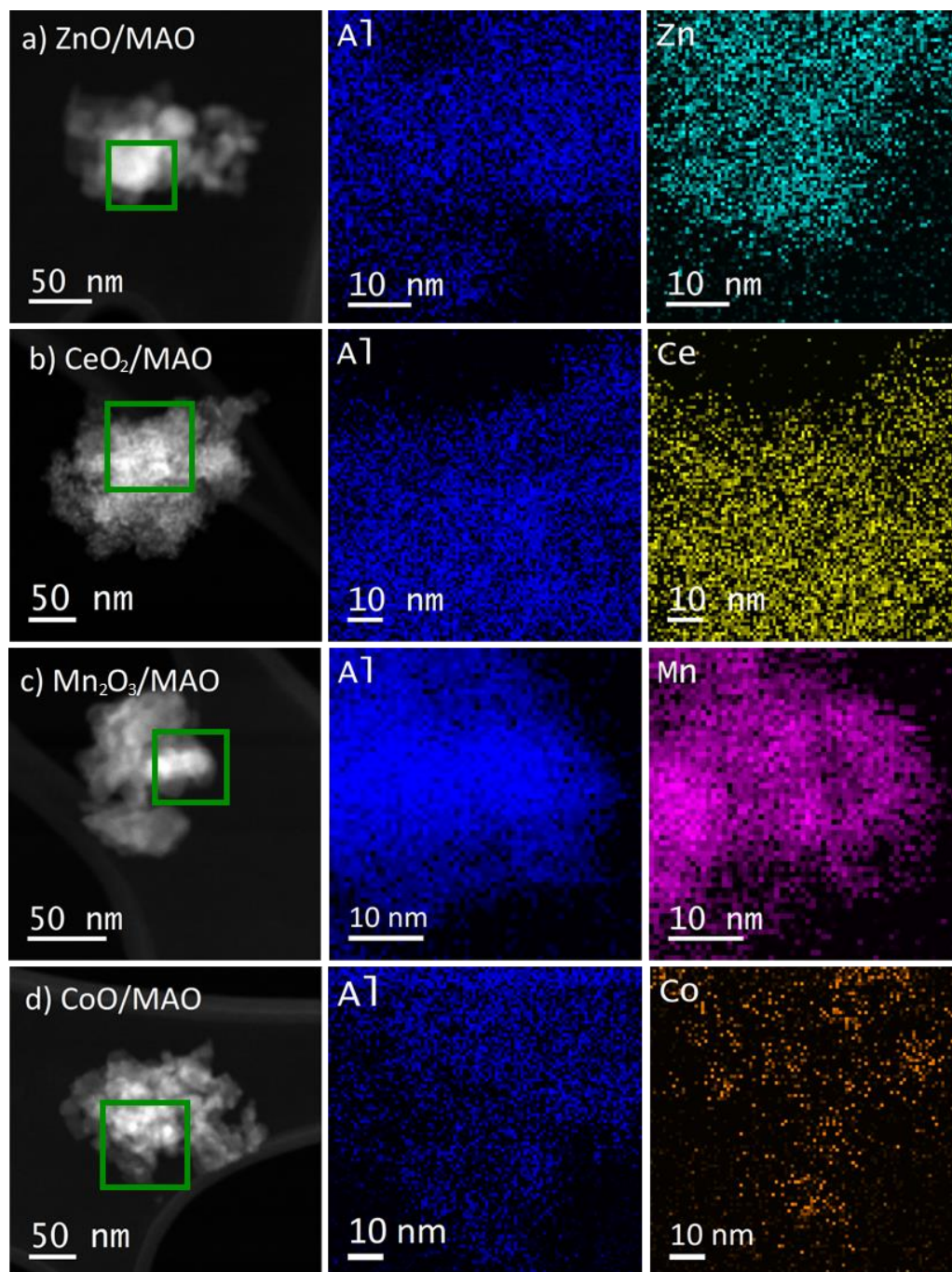


Figure 2. High angle annular dark field STEM images and EDS maps taken from the regions in green boxes for the ALD-modified supports (a) ZnO/MAO, (b) CeO₂/MAO, (c) Mn₂O₃/MAO, (d) CoO/MAO.

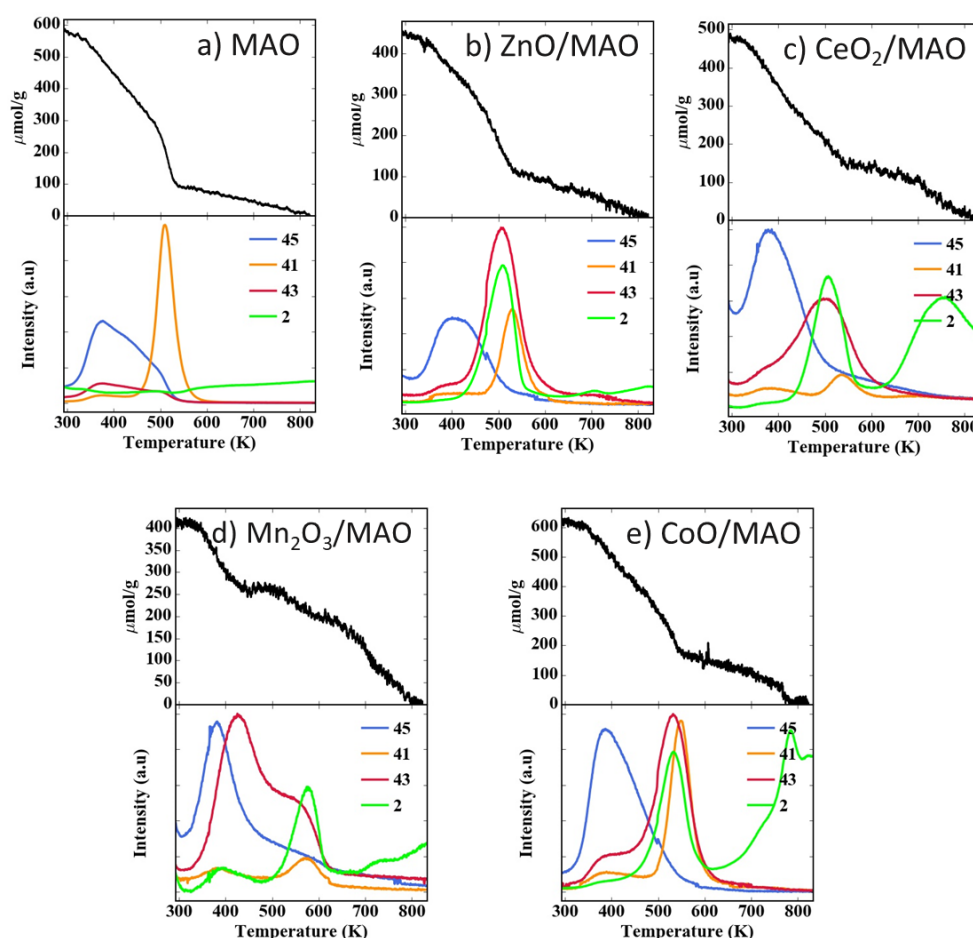


Figure 3. Temperature programmed desorption (TPD) and thermogravimetric analysis (TGA) results for 2-propanol on the supports used in this study, (a) MAO, (b) ZnO/MAO, (c) CeO₂/MAO, (d) Mn₂O₃/MAO, (e) CoO/MAO. Characteristic mass fragments: 2-propanol ($m/e = 45$), propene ($m/e = 41$), and acetone ($m/e = 43$).

The TPD-TGA data for each of the ALD-modified supports are significantly different, as shown in Figure 3b,e. The specific saturation coverages following evacuation were again similar to the value found on MAO, ranging from 3.2 to 4.9×10^{18} molecules/m²; again, about half of the adsorbed 2-propanol left each surface unreacted at lower temperatures. With ZnO/MAO, the main products were acetone ($m/e = 43$) and H₂ ($m/e = 2$) at 500 K, with a propene shoulder at higher temperatures. Results for CeO₂/MAO and CoO/MAO were similar to that found on ZnO/MAO except that acetone formed over a broader temperature range and some H₂ did not leave the surface until above 650 K. Finally, a much higher fraction of the 2-propanol desorbed as acetone on Mn₂O₃/MAO, beginning at temperatures below 400 K. For purposes of this study, the most important point is that the sharp propene peak at 500 K that was observed on MAO was completely absent on all of the ALD-modified supports. If patches of MAO had remained uncovered by the oxide overlayers, one would expect to see reaction of the 2-propanol at that temperature [38].

2.2. Water–Gas–Shift Measurements

To establish the most effective method for depositing Cu onto the various supports, we first examined two Cu/MAO catalysts in which Cu was added by either conventional impregnation (impCu/MAO) or by one ALD cycle of the Cu precursor (Cu/MAO). After calcination at 773 K, both catalysts were reduced in flowing H₂ at 623 K. Some properties of these catalysts are shown in Table 2. The dispersion, determined by N₂O adsorption, was approximately two times higher on the ALD-prepared catalyst, 15% versus 8%, resulting in

a calculated particle size that was a factor of almost two smaller, 7 nm versus 13 nm. The TEM images of the two catalysts in Figure 4a,b agreed well with the particle-size estimates obtained by N₂O adsorption.

Table 2. Weight loadings, dispersions, and equivalent particle sizes of various samples.

Sample	Weight Loading (%)	Dispersion (%)	Particle Size (nm)
Cu/MAO	1.1	15	7
impCu/MAO	1.0	8	13
Cu/MAO (1073K) *	1.1	6.5	17
Cu/ZnO/MAO	1.0	–	–
Cu/CeO ₂ /MAO	0.9	–	–
Cu/Mn ₂ O ₃ /MAO	1.0	–	–
Cu/CoO/MAO	1.1	–	–

* All samples were reduced at 623 K except for Cu/MAO (1073K) which was reduced at 1073 K.

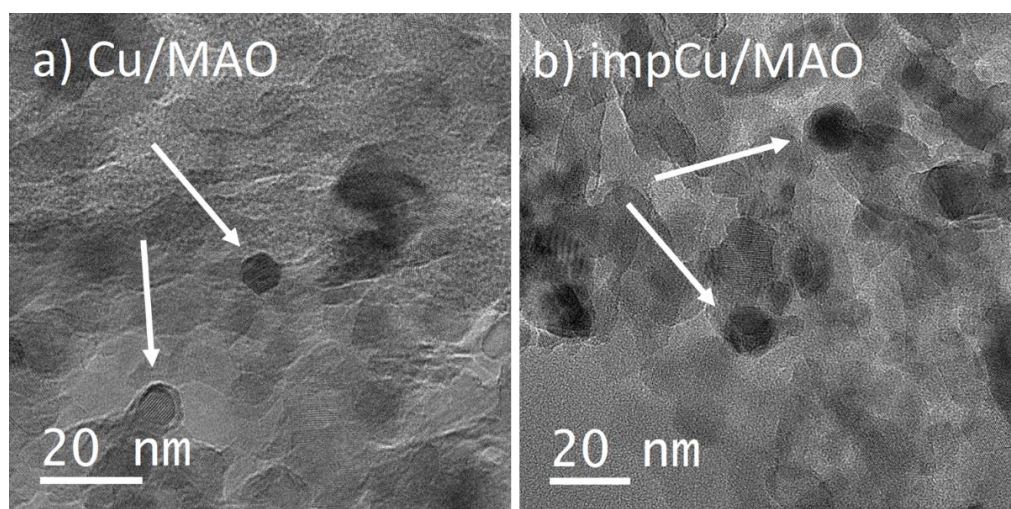


Figure 4. TEM images of (a) Cu/MAO and (b) impCu/MAO. Cu particles are shown by the arrows.

Figure 5a reports Arrhenius plots of the WGS rates on these two Cu/MAO catalysts. The activation energies determined from the slopes of the two lines on this plot are similar, 33.4 kJ/mol and 36.7 kJ/mol; however, the absolute rates differed by a factor of approximately 10. This difference in rates was five times greater than the difference in Cu surface areas, implying that the reaction must be structure sensitive. Literature reports concerning the structure sensitivity of WGS over Cu show disagreements [4]. At least one report concluded that the reaction is strictly proportional to the exposed area of Cu [39], while another report found that the turnover frequency did change with Cu loading, possibly due to micro-strain or the presence of Zn cations [40]. WGS rates on the MAO itself were undetectable between 423 K and 623 K.

In our examination of the effects of the support, Cu was added to the MAO-supported films using one ALD cycle of the Cu precursor, so that the structure of the particles would be similar. In addition to ensuring that all catalysts were prepared in the same manner, adding Cu by vapor-phase methods also avoided having to immerse the supports into a solvent, which could potentially dissolve and modify the structure of the oxide films. The Cu loadings after one ALD cycle, shown in Table 2, were slightly lower than that of the Cu/MAO catalyst because the surface areas of the supports were slightly lower; however, the coverages were between 1 and 2×10^{18} Cu atoms/m² in all cases, consistent with a constant growth rate in the ALD process.

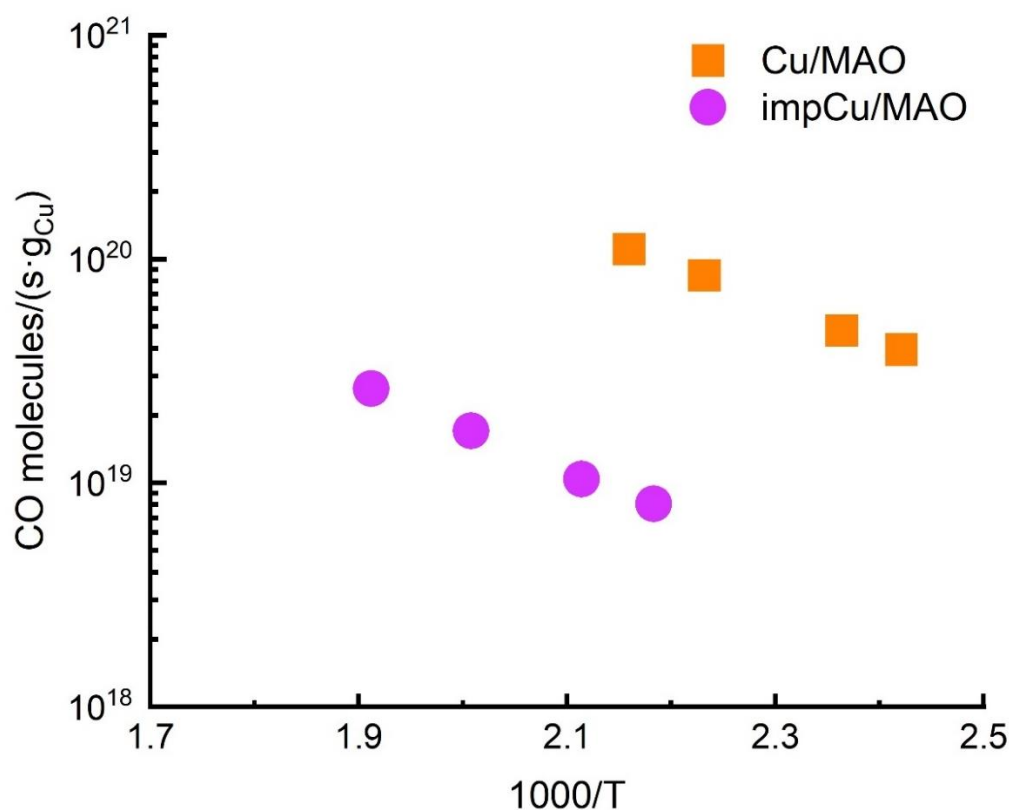


Figure 5. Differential WGS rates on Cu/MAO and impCu/MAO catalysts after reduction at 623 K.

WGS reaction rates were initially measured following oxidation of the ALD-prepared catalysts at 773 K and a low reduction temperature of 623 K. Oxidation at 773 K was necessary to remove the precursor ligands, while reduction at 623 K was sufficiently low to minimize sintering. The differential, WGS reaction rates for each of these catalysts are shown in Figure 6a. With the possible exception of the Cu/CoO/MAO catalyst, rates on each of the other catalysts on ALD-modified supports were identical, with identical activation energies, within experimental uncertainty. Rates on Cu/CoO/MAO also showed the same activation energy but were shifted downward by a factor of about three. Although cobalt oxide is normally not reduced to its metallic state by the mild conditions used in this study, the zero-valent state is the thermodynamically stable form of cobalt under WGS conditions [29]. It is possible that the lower rates on Cu/CoO/MAO are due to partial reduction of the support and deactivation of some of the Cu due to formation of a less reactive Cu-Co alloy. All of the other oxide films will remain oxides under the conditions of these experiments. An obvious conclusion of Figure 6a is that the support composition has no influence on the WGS reaction rates over Cu.

Support interactions can also stabilize the metal dispersion in heterogeneous catalysts, and Cu catalysts are highly susceptible to sintering. To determine whether the various oxide films could affect Cu stability, each of the ALD-prepared Cu catalysts were reduced at 1073 K for 1 h in flowing H₂, after which the differential WGS rates were again measured. These rates are shown in Figure 6b. A brief reduction at 1073 K, a temperature significantly above the Tamman temperature of Cu, 678 K, was chosen in order to simulate what would happen after long-time aging. After the high-temperature treatment, rates on Cu/MAO and Cu/ZnO/MAO dropped by a factor of about 10. In the case of Cu/MAO, the N₂O-measured dispersion dropped from 15% to 6.5% (See Table 2), implying that the loss in activity cannot be entirely explained by a loss in Cu dispersion. Apparently, high-temperature reduction also changes the structure of the Cu particles, resulting in some lost activity. The similarity between Cu/MAO and Cu/ZnO/MAO suggests that ZnO does not have a dramatic effect on the WGS rates. Some mild stabilization was observed with

Cu/CeO₂/MAO and Cu/Mn₂O₃/MAO. Both CeO₂ and Mn₂O₃ are partially reduced by heating in H₂ at 1073 K and the reduced oxides likely suppress Cu sintering. Interestingly, high-temperature reduction had very little effect on Cu/CoO/MAO. This is possibly consistent with alloy formation, since Co has a much higher melting temperature than Cu.

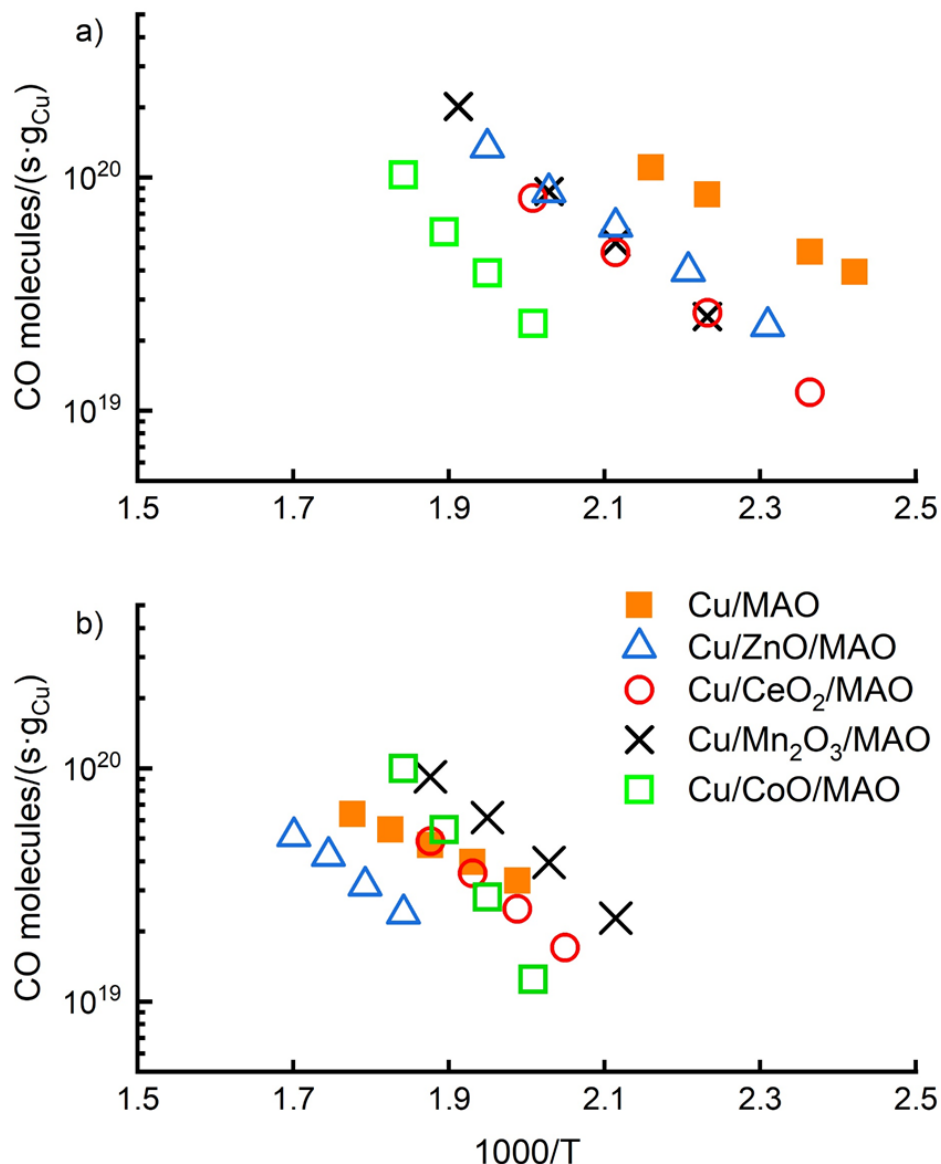


Figure 6. Differential WGS rates on catalysts reduced at (a) 623 K and (b) 1073 K.

The fact that commercial, low-temperature, WGS catalysts incorporate ZnO and other promoters into their catalysts implies that these additives provide advantages under realistic, industrial conditions [4]. What the results of our present work suggest is that these advantages are likely not due to a simple promotion of the catalytic properties of Cu. We have already noted that ZnO can act as a sulfur getter to protect Cu [4,16]; given that these catalysts are often prepared by co-precipitation of Cu, Al₂O₃, and ZnO, with much higher Cu loadings, it is also possible that the promoters affect rates by changing the structure of the Cu particles. As also noted earlier, the WGS reaction appears to be structure sensitive on Cu. This leads to an important conclusion. If the key to better catalysts involves modifying the structure of the metal particles, the strategy for preparing and stabilizing Cu catalysts needs to incorporate ways to change the structure of the metal particles.

Finally, the work shown here demonstrates the utility of using ALD modification to study support effects in metal catalysts. ALD modification of supports allows preparation

of supports in which the composition of the surface can be varied while maintaining surface area and pore size relatively constant. For reactions in which the surface texture plays a role, maintaining that texture may not be possible in other ways.

3. Materials and Methods

The inert support used in this study, MgAl_2O_4 (MAO, Puralox MG 26/100, Sasol, Hamburg, Germany), was calcined at 1173 K prior to use in order to ensure that its surface area would not change during the course of these experiments. Oxide films were deposited onto the MAO by ALD using procedures and equipment that are described in more detail elsewhere [41]. Briefly, ~0.4-g samples were evacuated using a mechanical pump and then exposed to a few torr of the desired precursor for 5 min at 553 K. After evacuation, the samples were removed from the system and placed in a muffle furnace for 5 min at 773 K to remove the precursor ligands. This procedure was repeated 20 times for each of the oxide films studied here. The precursors used in this study were all obtained from Strem Chemicals, Inc., and included bis(2,2,6,6-tetramethyl-3,5-heptanedionato)copper(II) 99% [$\text{Cu}(\text{TMHD})_2$], tris(2,2,6,6-tetramethyl-3,5-heptanedionato)manganese(III) 99% [$\text{Mn}(\text{TMHD})_3$], tetrakis(2,2,6,6-tetramethyl-3,5-heptanedionato)cerium(IV) min. 97% (99.9%-Ce) (REO) [$\text{Ce}(\text{TMHD})_4$], bis(2,2,6,6-tetramethyl-3,5-heptanedionato)zinc 99% [$\text{Zn}(\text{TMHD})_2$], and tris(2,2,6,6-tetramethyl-3,5-heptanedionato)cobalt(III) 99% (99.9+%-Co) [$\text{Co}(\text{TMHD})_3$].

Support interactions are expected to be most important for small metal particles [30]; therefore, we chose to examine only catalysts with low Cu loadings of roughly 1-wt%. The weight loading was determined gravimetrically. For most of the samples in this study, Cu was added to the supports using one ALD cycle with the Cu precursor ($\text{Cu}(\text{TMHD})_2$), followed by calcination at 773 K. Addition of metals by ALD has been shown to maximize the dispersion of metal catalysts in other cases [42]. However, to determine the effect of preparation methods, an MAO-supported Cu catalyst was also synthesized by impregnation with an aqueous solution of $\text{Cu}(\text{NO}_3)_2$ (99%, Sigma-Aldrich, St. Louis, MO, USA). After adding the $\text{Cu}(\text{NO}_3)_2$, the sample prepared by impregnation was dried in an oven at 333 K overnight, then calcined in a muffle furnace at 723 K.

BET surface areas were measured in a home-built apparatus using N_2 adsorption at 77 K. Transmission Electron Microscopy (TEM), Scanning Transmission Electron Microscopy (STEM) and Energy Dispersive X-ray Spectroscopy (EDS) were obtained on selected samples using a JEOL F200 scanning/transmission electron microscope, purchased from JEOL USA, Inc., Peabody, MA, USA. The Cu dispersions on the MAO supports were estimated using N_2O adsorption, using the following procedure [43]. First, 0.5-g samples were reduced in flowing H_2 (20 mL/min) at 623 K for 1 h, then cooled to 333 K in flowing He. After this, the sample was exposed to flowing N_2O (1.6 mL/min) to oxidize the surface of the Cu to Cu_2O without oxidizing the bulk. After purging any remaining N_2O with He, the sample was exposed to flowing CO (2.25 mL/min) while ramping the temperature from 333 K to 623 K at a rate of 30 K/min. The amount of CO_2 produced was quantified using a quadrupole mass spectrometer (Stanford Research Systems, RGA-100, Sunnyvale, CA, USA) and used to calculate the amount of surface Cu. Unfortunately, it was not possible to measure Cu dispersions by N_2O reaction on catalysts containing reducible oxides due to reaction with the oxide films.

Previous work has shown that the temperature at which 2-propanol reacts in Temperature Programmed Desorption (TPD)/Thermogravimetric Analysis (TGA) experiments is very sensitive to the surface composition [38,44]. TPD-TGA with 2-propanol were performed with 20-mg samples in a turbo-pumped vacuum system that is described elsewhere [42]. After heating a sample in vacuum at 823 K, it was cooled to room temperature, exposed to 10 torr of 2-propanol for several minutes, and then evacuated for 1 h. TPD-TGA measurements were obtained while heating the evacuated sample at 10 K/min, using a microbalance (Cahn 2000, Cerritos, CA, USA) to measure the mass changes and mass

spectrometer to measure the gas phase (Stanford Research Systems, RGA-100, Sunnyvale, CA, USA).

The WGS reactions were conducted in a $\frac{1}{4}$ " quartz tubular flow reactor. Approximately 0.1-g samples were placed in the center of the quartz tube and heated in a tubular furnace. CO and H₂O were fed to the reactor at partial pressures of 25 torr, using He as the balance. The total gas flowrate was 64.3 mL/min and all lines were heated to avoid condensation. The product stream was analyzed using a gas chromatograph (SRI Model 8610C, Torrance, CA, USA) equipped with a Haysep Q column. Each rate measurement was performed several times to ensure reproducibility. For the construction of the Arrhenius plots, conversions were always kept below 15% to ensure differential conditions.

4. Conclusions

Reaction rates for the WGS reaction on supported-Cu catalysts with low Cu loadings on MAO and MAO modified with thin films of ZnO, CeO₂, Mn₂O₃, and CoO suggest that the reaction on Cu is sensitive to the Cu structure but is not sensitive to the composition of the support. This has potential implications for the preparation of improved low-temperature WGS catalysts.

Author Contributions: Conceptualization, R.J.G. and J.M.V.; methodology, J.C.; validation, R.J.G. and J.M.V.; formal analysis, R.J.G., J.M.V. and J.C.; investigation, J.C. and Z.F.; resources, R.J.G. and J.M.V.; data curation, R.J.G., J.M.V. and J.C.; writing—original draft preparation, J.C.; writing—review and editing, R.J.G., J.M.V. and J.C.; visualization, J.C.; supervision, R.J.G. and J.M.V.; project administration, R.J.G. and J.M.V.; funding acquisition, R.J.G., J.M.V. and J.C. All authors have read and agreed to the published version of the manuscript.

Funding: This research was funded by the Vagelos Institute for Energy Science Technology at the University of Pennsylvania and by the Catalysis Center for Energy Innovation, an Energy Frontier Research Center funded by the U.S. Department of Energy, Office of Science, Office of Basic Energy Sciences under Award number DE-SC0001004.

Data Availability Statement: Data are contained within the article.

Conflicts of Interest: The authors declare no conflict of interest. The funders had no role in the design of the study; in the collection, analyses, or interpretation of data; in the writing of the manuscript; or in the decision to publish the results.

References

1. Bartholomew, C.H.; Farrauto, R.J. Hydrogen Production and Synthesis Gas Reactions. In *Fundamentals of Industrial Catalytic Processes*; John Wiley and Sons: Hoboken, NJ, USA, 2005; pp. 339–486.
2. Opalka, S.M.; Vanderspurt, T.H.; Radhakrishnan, R.; She, Y.; Willigan, R.R. Design of Water Gas Shift Catalysts for Hydrogen Production in Fuel Processors. *J. Phys. Condens. Matter* **2008**, *20*, 64237. [[CrossRef](#)]
3. Yaccato, K.; Carhart, R.; Hagemeyer, A.; Herrmann, M.; Lesik, A.; Strasser, P.; Volpe, A.; Turner, H.; Weinberg, H.; Grasselli, R.K.; et al. High Throughput Discovery of Families of High Activity WGS Catalysts: Part I—History and Methodology. *Comb. Chem. High Throughput Screen.* **2010**, *13*, 318–330. [[CrossRef](#)]
4. Ratnasamy, C.; Wagner, J.P. Water Gas Shift Catalysis. *Catal. Rev.* **2009**, *51*, 325–440. [[CrossRef](#)]
5. Bunluesin, T.; Gorte, R.J.; Graham, G.W. Studies of the Water-Gas-Shift Reaction on Ceria-Supported Pt, Pd, and Rh: Implications for Oxygen-Storage Properties. *Appl. Catal. B Environ.* **1998**, *15*, 107–114. [[CrossRef](#)]
6. Deshpande, P.A.; Madras, G. Support-Dependent Activity of Noble Metal Substituted Oxide Catalysts for the Water Gas Shift Reaction. *AIChE J.* **2010**, *56*, 2662–2676. [[CrossRef](#)]
7. Han, W.-Q.; Wen, W.; Hanson, J.C.; Teng, X.; Marinkovic, N.; Rodriguez, J.A. One-Dimensional Ceria as Catalyst for the Low-Temperature Water–Gas Shift Reaction. *J. Phys. Chem. C* **2009**, *113*, 21949–21955. [[CrossRef](#)]
8. Kinch, R.T.; Cabrera, C.R.; Ishikawa, Y. A Density-Functional Theory Study of the Water–Gas Shift Mechanism on Pt/Ceria(111). *J. Phys. Chem. C* **2009**, *113*, 9239–9250. [[CrossRef](#)]
9. Meira, D.M.; Ribeiro, R.U.; Mathon, O.; Pascarelli, S.; Bueno, J.M.C.; Zanchet, D. Complex Interplay of Structural and Surface Properties of Ceria on Platinum Supported Catalyst under Water Gas Shift Reaction. *Appl. Catal. B Environ.* **2016**, *197*, 73–85. [[CrossRef](#)]
10. González, I.D.; Navarro, R.M.; Wen, W.; Marinkovic, N.; Rodríguez, J.A.; Rosa, F.; Fierro, J.L.G. A Comparative Study of the Water Gas Shift Reaction over Platinum Catalysts Supported on CeO₂, TiO₂ and Ce-Modified TiO₂. *Catal. Today* **2010**, *149*, 372–379. [[CrossRef](#)]

11. Kalamaras, C.M.; Panagiotopoulou, P.; Kondarides, D.I.; Efstathiou, A.M. Kinetic and Mechanistic Studies of the Water–Gas Shift Reaction on Pt/TiO₂ Catalyst. *J. Catal.* **2009**, *264*, 117–129. [[CrossRef](#)]
12. Azzam, K.G.; Babich, I.V.; Seshan, K.; Lefferts, L. Bifunctional Catalysts for Single-Stage Water–Gas Shift Reaction in Fuel Cell Applications.: Part 1. Effect of the Support on the Reaction Sequence. *J. Catal.* **2007**, *251*, 153–162. [[CrossRef](#)]
13. Shah, P.R.; Kim, T.; Zhou, G.; Fornasiero, P.; Gorte, R.J. Evidence for Entropy Effects in the Reduction of Ceria–Zirconia Solutions. *Chem. Mater.* **2006**, *18*, 5363–5369. [[CrossRef](#)]
14. Gokhale, A.A.; Dumesic, J.A.; Mavrikakis, M. On the Mechanism of Low-Temperature Water Gas Shift Reaction on Copper. *J. Am. Chem. Soc.* **2008**, *130*, 1402–1414. [[CrossRef](#)] [[PubMed](#)]
15. Colussi, S.; Katta, L.; Amoroso, F.; Farrauto, R.J.; Trovarelli, A. Ceria-Based Palladium Zinc Catalysts as Promising Materials for Water Gas Shift Reaction. *Catal. Commun.* **2014**, *47*, 63–66. [[CrossRef](#)]
16. Pal, D.B.; Chand, R.; Upadhyay, S.N.; Mishra, P.K. Performance of Water Gas Shift Reaction Catalysts: A Review. *Renew. Sustain. Energy Rev.* **2018**, *93*, 549–565. [[CrossRef](#)]
17. Yu, W.-Z.; Wang, W.-W.; Ma, C.; Li, S.-Q.; Wu, K.; Zhu, J.-Z.; Zhao, H.-R.; Yan, C.-H.; Jia, C.-J. Very High Loading Oxidized Copper Supported on Ceria to Catalyze the Water-Gas Shift Reaction. *J. Catal.* **2021**, *402*, 83–93. [[CrossRef](#)]
18. Curran, C.D.; Lu, L.; Kiely, C.J.; McIntosh, S. Ambient Temperature Aqueous Synthesis of Ultrasmall Copper Doped Ceria Nanocrystals for the Water Gas Shift and Carbon Monoxide Oxidation Reactions. *J. Mater. Chem. A* **2018**, *6*, 244–255. [[CrossRef](#)]
19. Rodríguez, J.A.; Evans, J.; Graciani, J.; Park, J.-B.; Liu, P.; Hrbek, J.; Sanz, J.F. High Water–Gas Shift Activity in TiO₂(110) Supported Cu and Au Nanoparticles: Role of the Oxide and Metal Particle Size. *J. Phys. Chem. C* **2009**, *113*, 7364–7370. [[CrossRef](#)]
20. Boisen, A.; Janssens, T.V.W.; Schumacher, N.; Chorkendorff, I.; Dahl, S. Support Effects and Catalytic Trends for Water Gas Shift Activity of Transition Metals. *J. Mol. Catal. A Chem.* **2010**, *315*, 163–170. [[CrossRef](#)]
21. Franchini, C.A.; de Farias, A.M.D.; Albuquerque, E.M.; dos Santos, R.; Fraga, M.A. Single-Stage Medium Temperature Water-Gas Shift Reaction over Pt/ZrO₂—Support Structural Polymorphism and Catalyst Deactivation. *Appl. Catal. B Environ.* **2012**, *117–118*, 302–309. [[CrossRef](#)]
22. Djinić, P.; Batista, J.; Pintar, A. Calcination Temperature and CuO Loading Dependence on CuO-CeO₂ Catalyst Activity for Water-Gas Shift Reaction. *Appl. Catal. A Gen.* **2008**, *347*, 23–33. [[CrossRef](#)]
23. Si, R.; Raitano, J.; Yi, N.; Zhang, L.; Chan, S.-W.; Flytzani-Stephanopoulos, M. Structure Sensitivity of the Low-Temperature Water-Gas Shift Reaction on Cu–CeO₂ Catalysts. *Catal. Today* **2012**, *180*, 68–80. [[CrossRef](#)]
24. Tanaka, Y.; Utaka, T.; Kikuchi, R.; Sasaki, K.; Eguchi, K. Water Gas Shift Reaction over Cu-Based Mixed Oxides for CO Removal from the Reformed Fuels. *Appl. Catal. A Gen.* **2003**, *242*, 287–295. [[CrossRef](#)]
25. Tabakova, T.; Idakiev, V.; Avgouropoulos, G.; Papavasiliou, J.; Manzoli, M.; Boccuzzi, F.; Ioannides, T. Highly Active Copper Catalyst for Low-Temperature Water-Gas Shift Reaction Prepared via a Cu-Mn Spinel Oxide Precursor. *Appl. Catal. A Gen.* **2013**, *451*, 184–191. [[CrossRef](#)]
26. Ávila-Neto, C.N.; Zanchet, D.; Hori, C.E.; Ribeiro, R.U.; Bueno, J.M.C. Interplay between Particle Size, Composition, and Structure of MgAl₂O₄-Supported Co–Cu Catalysts and Their Influence on Carbon Accumulation during Steam Reforming of Ethanol. *J. Catal.* **2013**, *307*, 222–237. [[CrossRef](#)]
27. White, E.C.; Shultz, J.F. Fused Cobalt Oxide as a Water Gas Catalyst. *Ind. Eng. Chem.* **1934**, *26*, 95–97. [[CrossRef](#)]
28. Wang, J.; Chernavskii, P.A.; Khodakov, A.Y.; Wang, Y. Structure and Catalytic Performance of Alumina-Supported Copper–Cobalt Catalysts for Carbon Monoxide Hydrogenation. *J. Catal.* **2012**, *286*, 51–61. [[CrossRef](#)]
29. Bakhmutsky, K.; Wiedner, N.L.; Baldassare, T.; Smith, M.A.; Gorte, R.J. A Thermodynamic Study of the Redox Properties of Supported Co Particles. *Appl. Catal. A Gen.* **2011**, *397*, 266–271. [[CrossRef](#)]
30. Ro, I.; Resasco, J.; Christopher, P. Approaches for Understanding and Controlling Interfacial Effects in Oxide-Supported Metal Catalysts. *ACS Catal.* **2018**, *8*, 7368–7387. [[CrossRef](#)]
31. Vesborg, P.C.K.; Chorkendorff, I.; Knudsen, I.; Balmes, O.; Nerlov, J.; Molenbroek, A.M.; Clausen, B.S.; Helveg, S. Transient Behavior of Cu/ZnO-Based Methanol Synthesis Catalysts. *J. Catal.* **2009**, *262*, 65–72. [[CrossRef](#)]
32. Chen, C.S.; Lai, Y.T.; Lai, T.W.; Wu, J.H.; Chen, C.H.; Lee, J.F.; Kao, H.M. Formation of Cu Nanoparticles in SBA-15 Functionalized with Carboxylic Acid Groups and Their Application in the Water–Gas Shift Reaction. *ACS Catal.* **2013**, *3*, 667–677. [[CrossRef](#)]
33. Roberts, S.; Gorte, R.J. A Comparison of Pt Overlayers on α -Al₂O₃(0001), ZnO(0001)Zn, and ZnO(0001⁻)O. *J. Chem. Phys.* **1990**, *93*, 5337–5344. [[CrossRef](#)]
34. Onn, T.M.; Zhang, S.; Arroyo-Ramirez, L.; Xia, Y.; Wang, C.; Pan, X.; Graham, G.W.; Gorte, R.J. High-Surface-Area Ceria Prepared by ALD on Al₂O₃ Support. *Appl. Catal. B Environ.* **2017**, *201*, 430–437. [[CrossRef](#)]
35. Mao, X.; Foucher, A.; Stach, E.A.; Gorte, R.J. A Study of Support Effects for CH₄ and CO Oxidation over Pd Catalysts on ALD-Modified Al₂O₃. *Catal. Lett.* **2019**, *149*, 905–915. [[CrossRef](#)]
36. Miikkulainen, V.; Leskelä, M.; Ritala, M.; Puurunen, R.L. Crystallinity of Inorganic Films Grown by Atomic Layer Deposition: Overview and General Trends. *J. Appl. Phys.* **2013**, *113*, 21301. [[CrossRef](#)]
37. Lin, C.; Foucher, A.C.; Ji, Y.; Curran, C.D.; Stach, E.A.; McIntosh, S.; Gorte, R.J. “Intelligent” Pt Catalysts Studied on High-Surface-Area CaTiO₃ Films. *ACS Catal.* **2019**, *9*, 7318–7327. [[CrossRef](#)]
38. Wang, C.; Mao, X.; Lee, J.D.; Onn, T.M.; Yeh, Y.-H.; Murray, C.B.; Gorte, R.J. A Characterization Study of Reactive Sites in ALD-Synthesized WO_x/ZrO₂ Catalysts. *Catalysts* **2018**, *8*, 292. [[CrossRef](#)]

39. Ginés, M.J.L.; Amadeo, N.; Laborde, M.; Apesteguía, C.R. Activity and Structure-Sensitivity of the Water-Gas Shift Reaction over CuZnAl Mixed Oxide Catalysts. *Appl. Catal. A Gen.* **1995**, *131*, 283–296. [[CrossRef](#)]
40. Chinchén, G.C.; Spencer, M.S. Sensitive and Insensitive Reactions on Copper Catalysts: The Water-Gas Shift Reaction and Methanol Synthesis from Carbon Dioxide. *Catal. Today* **1991**, *10*, 293–301. [[CrossRef](#)]
41. Cao, T.; Kwon, O.; Lin, C.; Vohs, J.M.; Gorte, R.J. Two-Dimensional Perovskite Crystals Formed by Atomic Layer Deposition of CaTiO₃ on γ -Al₂O₃. *Nanomaterials* **2021**, *11*, 2207. [[CrossRef](#)]
42. Huang, R.; Cheng, Y.; Ji, Y.; Gorte, R.J. Atomic Layer Deposition for Preparing Isolated Co Sites on SiO₂ for Ethane Dehydrogenation Catalysis. *Nanomaterials* **2020**, *10*, 244. [[CrossRef](#)] [[PubMed](#)]
43. Dandekar, A.; Vannice, M.A. Determination of the Dispersion and Surface Oxidation States of Supported Cu Catalysts. *J. Catal.* **1998**, *178*, 621–639. [[CrossRef](#)]
44. Onn, T.M.; Küngas, R.; Fornasiero, P.; Huang, K.; Gorte, R.J. Atomic Layer Deposition on Porous Materials: Problems with Conventional Approaches to Catalyst and Fuel Cell Electrode Preparation. *Inorganics* **2018**, *6*, 34. [[CrossRef](#)]